



# Detection, size characterization and quantification of silver nanoparticles in consumer products by particle collision coulometry

Deamelys Hernández<sup>1</sup> · Juan C. Vidal<sup>1</sup> · Francisco Laborda<sup>1</sup> · Josefina Pérez-Arantegui<sup>1</sup> · Ana C. Giménez-Ingalaturre<sup>1</sup> · Juan R. Castillo<sup>1</sup>

Received: 14 July 2020 / Accepted: 20 November 2020 / Published online: 3 January 2021  
© Springer-Verlag GmbH Austria, part of Springer Nature 2021

## Abstract

Silver nanoparticles (AgNPs) are widely used in industrial and consumer products owing to its antimicrobial nature and multiple applications. Consequently, their release into the environment is becoming a big concern because of their negative impacts on living organisms. In this work, AgNPs were detected at a potential of + 0.70 V vs. Ag/AgCl reference electrode, characterized, and quantified in consumer products by particle collision coulometry (PCC). The electrochemical results were compared with those measured with electron microscopy and single-particle inductively coupled plasma mass spectrometry. The theoretical and practical peculiarities of the application of PCC technique in the characterization of AgNPs were studied. Reproducible size distributions of the AgNPs were measured in a range 10–100 nm diameters. A power allometric function model was found between the frequency of the AgNPs collisions onto the electrode surface and the number concentration of nanoparticles up to a silver concentration of  $10^{10} \text{ L}^{-1}$  (ca.  $25 \text{ ng L}^{-1}$  for 10 nm AgNPs). A linear relationship between the number of collisions and the number concentration of silver nanoparticles was observed up to  $5 \times 10^7 \text{ L}^{-1}$ . The PCC method was applied to the quantification and size determination of the AgNPs in three-silver containing consumer products (a natural antibiotic and two food supplements). The mean of the size distributions (of the order 10–20 nm diameters) agrees with those measured by electron microscopy.

**Keywords** Silver nanoparticles · Particle collision coulometry · Single-particle inductively coupled plasma mass spectrometry · Scanning electron microscopy · Transmission electron microscopy · Nanoparticle size distribution

## Introduction

Silver nanoparticles (AgNPs) are extensively used and commercially applied in industrial, science (e.g., fabrication of biosensors), and biomedical applications [1]. This inevitably produces its ecological release in the environment during production, storage, and applications, causing toxicity and damaging effects after physical, chemical, and biological transformations [2]. Many studies evidence the toxicity of the AgNPs for mammalian cells, specially after releasing into the aquatic environments [3].

Exposure to AgNPs can occur from drinking, ingestion, inhalation, or through direct skin contact, which implies associated health risks. One of the important factors for preventing these risks is the availability of simpler and more suitable analytical techniques for the detection and characterization of nanoparticles at low concentrations in environment or consumer products. There is a correlation between toxicity and particle size, for example [4]. Other studies show that size, charge, and aggregation of nanoparticles in the medium are predictive of nanoparticle behavior, e.g., smaller nanoparticles with larger surface area, are excreted more easily from the body of living organisms [5].

Electron microscopy techniques, e.g., scanning electron microscopy (SEM) and transmission electron microscopy (TEM), are powerful high-resolution imaging techniques for obtaining size distributions of AgNPs, below 1 nm [6]. SEM and TEM images are easily interpreted, but the main drawback of electron microscopy is the aggregation/agglomeration of the silver nanoparticles during sample preparation, which

---

In memoriam of Prof. Juan R. Castillo

✉ Juan C. Vidal  
jcevidal@unizar.es

<sup>1</sup> Group of Analytical Spectroscopy and Sensors (GEAS), Institute of Environmental Sciences (IUCA), University of Zaragoza, c/ Pedro Cerbuna 12, 50009 Zaragoza, Spain

are involved in the removal of solvent and drying steps. In addition, the counting of nanoparticles in the analysis of the images is time-consuming and can be erroneous by the lack of contrast of small-sized nanoparticles [7].

The characterization of individual AgNPs has been extensively carried out by single-particle inductively coupled plasma mass spectrometry (SP-ICP-MS) [6, 8]. Very diluted suspensions of AgNPs are introduced into the plasma of the SP-ICP-MS instrument, where each nanoparticle produces a cloud of gaseous ions, which is recorded as an individual event by the mass spectrometer detector. The intensity of the events is related to the mass of silver in the particles, and hence to their size if the composition, density, and shape are known, whereas, the frequency of the events is proportional to the number concentration of nanoparticles. A typical SP-ICP-MS method gives information of mean sizes, size distributions, number, and mass concentration of nanoparticles.

Electrochemical techniques have also been used for the characterization of nanoparticles and nanotoxicity assessment, providing physical and chemical properties information, such as size distributions, number concentrations, aggregation or agglomeration states, diffusion coefficients, presence of molecular tags, electrocatalytics, or superficial oxidation states [6, 9, 10]. In particular, the electrochemical detection of direct or mediated single nanoparticle collisions on microelectrodes, by virtue of their random collision due to Brownian motion, allows to measuring their sizes, in the so-named particle collision coulometry (PCC), nanoparticle impact coulometry, or anodic particle coulometry [11–13]. Upon impacting the anodically potentiostated electrode, the AgNPs are oxidized producing small peaks of current. The magnitude of these peaks is related to the total number of atoms contained within the individual impacting nanoparticle, through the faradaic equivalence, hence providing information of size. The mathematical processing of the current peaks is a critical issue in the data obtained with the nano-impact methods, for example, the threshold to distinguish noise from faradaic currents, the use of Fourier transformations, or deconvolution from signals originated from the aggregation of the nanoparticles [14].

Additionally, the frequency of recorded impacts is related to the number concentration of the nanoparticles [12], although this technique has barely used with quantitative purposes. The nano-impact techniques have been thoroughly studied from a theoretical point of view, but their quantitative applications in samples are very scarce, limiting in very few cases to the detection of spiked AgNPs in seawater [15]. The quantification of ultralow concentration of nanoparticles is also possible by measuring the time of first arrival required to reach the electrode from random collisions, in the order of thousands of second. Femtomolar detection levels of AgNPs have been reported with this approach [16, 17]. The nano-impact electrochemical techniques have also been used for studying the solution-phase AgNPs agglomeration and aggregation [18].

In a similar way than SP-ICP-MS, PCC methods allow the rapid detection of nanoparticles (i.e., thousands of particles in less than a minute), while providing individual particle information of particles size, size distributions, and nanoparticle concentrations [6].

The aim of this work has been the application of the nano-impact coulometry for the detection, size characterization, and quantification of AgNPs in consumer products. The influence of the mathematical processing of the measured data on the results of size distributions is discussed. The quantifications and size distributions obtained with PCC were compared with those obtained with SP-ICP-MS and electron microscopy.

## Experimental

### Reagents

Citrate-capped AgNPs with a nominal diameter of 10, 20, 40, 60, and 100 nm ( $10.5 \pm 0.4$ ;  $20.0 \pm 1.2$ ;  $40.1 \pm 2.1$ ;  $58.9 \pm 6.1$ , and  $100.1 \pm 10.2$ ) were purchased from nanoComposix (San Diego, CA, USA) with a nominal silver concentration of  $20 \text{ mg L}^{-1}$ . Polyvinylpyrrolidone-coated AgNPs with a nominal diameter of 75 nm ( $74.6 \pm 3.8$  by TEM and  $69.2 \pm 0.9$  by SP-ICP-MS) were obtained from NIST (National Institute of Standards & Technology, Reference Material 8017). The stability of the AgNPs suspensions was monitored by UV-Visible spectroscopy through the strong plasmonic absorbance peak at about 400 nm (see Fig. S1 and Table S1 of the Electronic Supporting Material (ESM)). Sodium perchlorate monohydrated (98%,  $\text{NaClO}_4$ ) was supplied by Sigma-Aldrich (Madrid, Spain). Ultrapure water (Milli-Q Advantage, Molsheim, France) was used for dilutions (resistivity of  $18.2 \text{ M}\Omega \text{ cm}$  at 298 K).

Three consumer colloidal silver products, namely Biovedik™ (Alex Healthy and Natural Pvt. Ltd., Puducherry, India), Wellness™ Colloidal Silver (Source Naturals, Inc., Santa Cruz, USA), and High-Stability™ (Rivers of Health, Honiton, UK) were analyzed. These products are recommended as health products intended for internal usage or as surface sanitizers for external use (anti-microbial catalysts). Wellness™ is a colloidal silver supplement containing about  $30 \mu\text{g mL}^{-1}$  of silver stabilized with EDTA. Biovedik™ is commercialized as a natural antibiotic mix of ionic silver ( $>25 \mu\text{g mL}^{-1}$ ) and colloidal silver. High-Stability™ is a colloidal silver presented as a germicidal product with anti-bacterial, anti-viral, and anti-fungal properties. These samples were kept in a dark place at room temperature until analysis.

### Instrumentation

Electrochemical experiments were carried out with a PGSTAT-10 potentiostat (Metrohm Autolab BV, Utrecht,

The Netherlands, [www.metrohm-autolab.com](http://www.metrohm-autolab.com)) provided with an ECD low current module. This module gives a minimum current resolution of 0.3 fA, and is equipped with a built-in third-order Sallen-Key filter that helps to filter out noise. To reduce noise, the three electrodes were used inside a Faraday cage, and the connecting cables were specially shielded. A carbon fiber microelectrode ( $11 \pm 2 \mu\text{m}$  diameter), reference Ag/AgCl (3 M KCl), and Pt auxiliary electrodes were from BASi (BioAnalytical systems, [www.basinc.com](http://www.basinc.com)). The potentiostat was controlled by the NOVA v.2.1 electrochemical software (Metrohm). All experiments were conducted at  $20 \pm 3 \text{ }^\circ\text{C}$ .

A Perkin-Elmer NexION 2000B ICP mass spectrometer (Toronto, Canada) was used for SP-ICP-MS measurements. The sample introduction system consisted of a glass concentric nebulizer and a baffled cyclonic spray chamber. Samples were measured in single particle mode using the Syngistix Nano-Application module (PerkinElmer Inc.). The dwell times used was 100  $\mu\text{s}$  with a total acquisition time of 60 s.

A flame atomic absorption spectrometer (F-AAS) Analyst 200 (Perkin Elmer, Toronto, Canada), equipped with a silver hollow-cathode-lamp (operating current 2 mA, wavelength of 328.1 nm), was used for the determination in the samples of total silver, and ionic  $\text{Ag}^+$  in ultrafiltered samples (3 kDa pore size diameter).

TEM observations were carried out using a TEM system (Model 2000 FXII, JEOL, Tokyo, Japan), coupled with Energy Dispersive X-ray Spectrometry (EDS) and electron diffraction facilities, at 200 kV. Field-Emission Scanning Electron Microscopy (FESEM) and EDS analysis were performed with a Merlin<sup>TM</sup> FESEM equipped with a Gemini column (both from Carl Zeiss Nano Technology Systems, Jena, Germany, <https://www.zeiss.com/microscopy/int/home.html?vaURL=www.zeiss.com/nts>), and coupled with an X-Max X-Ray microanalyzer (Oxford Instruments, Abingdon, Oxfordshire, UK, [www.oxinst.com](http://www.oxinst.com)). FESEM images were recorded working at 5 kV with the in-Lens secondary-electron detector, in order to improve resolution, and EDS analyses were carried out at 10 kV.

### Nano-impact coulometry detection, size characterization, and determination of silver nanoparticles

The working carbon microelectrode was polished with alumina, rinsed with deionized water, sonicated in water for 3 min and rinsed again with deionized water, as previously reported [19]. All the glass materials and the electrochemical cells used were previously cleaned with *aqua regia* to ensure complete removal of silver, and the AgNPs dispersions were deoxygenated with nitrogen for about 60 s before measurements to preserve the chemical oxidative dissolution of silver and/or

the formation of silver oxide on nanoparticles by the presence of oxygen.

All the AgNPs dispersions were sonicated for 20 s immediately before being diluted or measured. Samples and standards of AgNPs (10, 40, 60, and 100 nm diameters) were diluted with supporting electrolyte (0.02 M  $\text{NaClO}_4$ ) up to a concentration of about  $25 \text{ ng L}^{-1}$  in a total volume of 10.0 mL. For the chronoamperometric measurements of these solutions in the three-electrode voltammetric cell, a  $-0.05 \text{ V}$  equilibration potential was held for 5 s and then currents were measured every 2.5 ms applying an anodic potential  $E_{\text{ox}} = +0.70 \text{ V}$  for 10 s with software NOVA v.2.1.4 (Metrohm Autolab BV, Utrecht, The Netherlands). The current spikes from the previous chronoamperograms, which are due to the collisions of the silver nanoparticles onto the working microelectrode surface, were subsequently analyzed with OriginPro 2020 v.9.7.0.188 software (OriginLab Corp., Northampton, MA, USA, [www.originlab.com](http://www.originlab.com)) as reported below. The spikes were identified automatically by this software after subtracting the baseline drift and applying an optimized threshold. Fourier transform filterings were studied for removing the electrical noise at 60 Hz and multiples up to 240 Hz.

### Characterization and quantification of silver nanoparticles in consumer products by SP-ICP-MS

Standards of AgNPs dispersions were prepared by accurately weighing aliquots of the stock dispersion. The Biovedick<sup>TM</sup> and High Stability<sup>TM</sup> samples were diluted into a silver concentration of about  $40 \text{ ng L}^{-1}$ , whereas the Wellness<sup>TM</sup> sample was diluted to about  $200 \text{ ng L}^{-1}$  of total silver. Standards and samples were diluted in ultrapure water, and all the silver suspensions were bath sonicated for 1 min before using. Calculations were performed within the Syngistix Nano-Application module (version 2.4). Nebulization efficiency was determined using ultra-uniform gold nanoparticle suspensions of  $47.8 \pm 1.8 \text{ nm}$  diameter (NanoComposix, San Diego, CA, USA). Sample flow rate was measured gravimetrically.

### Size characterization of silver nanoparticles in consumer products by electron microscopy

For TEM and FESEM examinations, samples were prepared by deposition of 20  $\mu\text{l}$  of the colloidal suspensions on carbon-coated copper grids, and then dried at room temperature. The colloidal suspensions were sonicated during 1 min, previously to deposition. Size distributions of the nanoparticles were measured using TEM and FESEM secondary-electron images. Average sizes and standard deviations (SD) were calculated by measuring over 150 nanoparticles in random regions of the images. The image analysis and size determinations were carried out using ImageJ software (version 1.52).

## Results and discussion

### PCC detection and size characterization of silver nanoparticles

The detection of the AgNPs was carried out via the particle collision coulometric (PCC) method. In very diluted suspensions, AgNPs diffuse freely due to Brownian motion and are voltammetrically detected due to stochastic impacts on the surface of a microelectrode. Upon impacting the microelectrode at a suitable potential, the AgNPs are oxidized resulting in small current-time transients (spikes) associated with the individual nanoparticles. The charge passed during the spike is quantitatively linked to the size of each nanoparticle, therefore extracting size distributions from the spike transients [20].

The experiences were carried out with very low concentrations of AgNPs (up to 25 ng L<sup>-1</sup>) to avoid aggregations or the simultaneous impact of two or more AgNPs on the working electrode. In these conditions, the oxidation of AgNPs allows to detect the individual silver nanoparticles. The faradaic of the current-transient spikes is related to the number of atoms of the AgNPs and hence their sizes. Microelectrodes were used to decrease capacitive currents and the adsorption of NPs on the electrode, allowing better resolution of the individual current transients.

Figure 1 shows a typical chronoamperogram from a deoxygenated solution of 20 ng L<sup>-1</sup> AgNPs in 0.02 M NaClO<sub>4</sub> supporting electrolyte. The inset (A) of the Fig. 1 represents in more detail the impact spikes of AgNPs. Collision events are sharp oxidative current peaks with durations of 5–10 ms in 0.02 M NaClO<sub>4</sub> supporting electrolyte. In blank solutions without nanoparticles, the spikes did not appear.

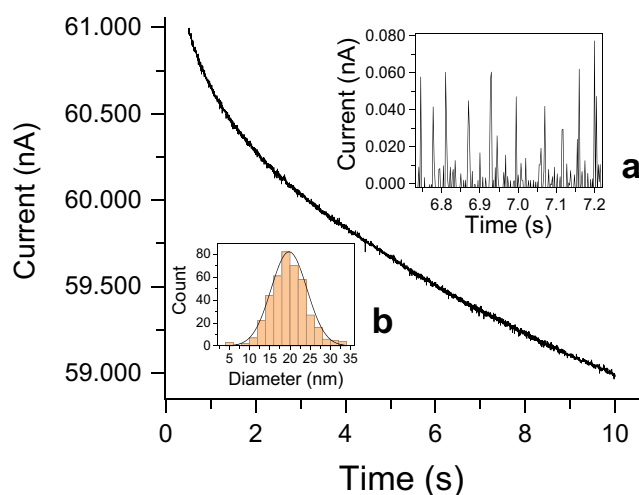


**Fig. 1** A typical chronoamperogram of a 20 ng L<sup>-1</sup> dispersion of AgNPs (20 nm diameter) in 0.02 M NaClO<sub>4</sub> recorded at  $E_a = +0.70$  V with a carbon fiber microelectrode. Inset (A): amplification showing the impact spikes between 6.7 and 7.2 s. Inset (B): a typical AgNPs size distribution calculated from the spikes recorded between 2 and 10 s

Assuming spherical AgNPs, the maximum charge passed from the complete oxidation of the particle (1 electron per atom) can be calculated through the Faraday's first law as [10]:

$$Q_{\max} = \frac{4F\pi\rho r_{\text{NP}}^3}{3A_r}$$

where  $F$  is the Faraday constant ( $F = 96,485.34$  C mol<sup>-1</sup>),  $\rho$  is the bulk density of silver (10.49 g cm<sup>-3</sup>),  $r_{\text{NP}}$  is the radius of the AgNP in cm, and  $A_r$  the relative atomic mass of silver (107.87). Using this equation, the diameter of the individual nanoparticles are calculated from the area of the current-transient peaks. A typical size distribution is shown in the inset (B) of Fig. 1.

### Mathematical treatment of PCC chronoamperograms

The current spikes were identified and integrated by using a mathematical treatment with the software OriginPro 2020. First, the drift of the chronoamperometric baseline was removed by asymmetric least squares smoothing, with an appropriate asymmetric factor (e.g., 0.20) and threshold values (e.g., 0.0001 nA). See additional information in the ESM.

The mathematical filtering of the currents by Fourier Transform to analyze the frequency spectrum of the baseline of the chronoamperograms did not show any improvement of the signals. This was probably due to the third-order Sallen-Key hardware filter of the ECD module used for measuring the currents [21]. In a second step, the faradaic current peaks were discriminated from the capacitive and noisy currents by using a threshold value (height values of about 0.0001 nA) before measuring the individual area of the peaks. The size distribution histograms were finally calculated after the automated filtering of the peaks under the selected criteria. In a real context, the threshold values were greatly dependent of the diameter of the AgNPs and the noise of the currents in the applied samples. For these reasons, care must be taken in order not to obtain erroneous results, and a correct optimization of these values were required. The values of these parameters were considered optimum once the smallest tailored size distribution of the silver nanoparticles was obtained. In this regard, additional information and results are given at the ESM. The influence of the asymmetric factor and threshold values on the calculated size distributions of nominal 20-nm AgNPs are shown in Fig. S3, S4, and S5 of the ESM, respectively.

### Optimization of the PCC procedure

Some experimental factors have a significant influence on the detection and proper size determinations of AgNPs, e.g., the particle-electrode contact time, the size of the NPs, and the kinetics of the faradaic process (i.e., the current peaks are

potential and domain-time dependents). The potential applied to the working electrode modifies the kinetics of the charge-transfer process. The duration of the single collision events was 5–10 ms, but the instrumental high-current Autolab ECD module that we used can take current measurements every 2.5 ms, which can limit the resolution of the resulted signals [21]. The timescale reflects the speed of the instrument electronics instead of the course of the nano-impact event. However, this contribution to the reproducibility was very small, as the results of size distributions were very similar by taking a resolution of 4 ms (data not shown).

The area of the currents peaks is related to the sizes of the nanoparticles through the Faraday first law equivalence, but only accurate results are obtained if the AgNPs are completely oxidized in the domain-time of the collision events. This is especially important for large AgNPs (diameters greater than 40 nm), where incomplete oxidation of the NPs can occur, especially in dependence on the substrate of the electrode and the kinetics of charge transfer. To study the influence of the oxidizing potential, AgNPs from 10 to 100 nm were oxidized at potentials of  $E_e = +0.50$  V and  $E_e = +0.70$  V vs. Ag/AgCl reference electrode. There were not significant differences ( $p = 0.05$ ) in the diameter of the 10 nm and 20 nm silver nanoparticles by applying a potential ( $E_e$ ) of +0.50 V and +0.70 V, due to the small size of these nanoparticles. However, for AgNPs of larger diameters (40, 60, and 100 nm), the potential of +0.5 V was insufficient to oxidize completely these nanoparticles during the collisions onto the electrode. The influence of the applied potential on the size distributions of the citrate capped AgNPs standards of 10–20–40–60–100 nm diameter is summarized in Fig. S6 of the ESM.

On the other hand, the capping agent also influenced on the oxidation kinetics of AgNPs with the working electrode [22]. The complete oxidation of the AgNP is the most important to obtain accurate results. For example, the polyvinylpyrrolidone (PVP) capped AgNPs of 75 nm diameter (NIST standard) were partial oxidized in the same experimental conditions of the citrate-capped standards ( $E_e = +0.700$  V), resulting in a calculated diameter of only  $42.0 \pm 8.2$  nm ( $n = 6$ ). The more insulating properties of the PVP-capped AgNPs comparing with citrate required a higher potential for their complete oxidation.

To minimize the capacitive and noise currents, it is well known that micrometer size electrodes are necessary in nano-impact electrochemistry experiences. Gold disc microelectrodes ( $500 \pm 50$   $\mu\text{m}$  diameter) showed higher current noise levels of  $\pm 6$  nA, compared to carbon fiber microelectrodes ( $11 \pm 2$   $\mu\text{m}$  diameter) with noise levels around  $\pm 0.001$  nA. Attempts to analyze impacts of AgNPs of 10 and 100 nm diameter with the Au disk minielectrode produced biased results, with diameters of  $100 \pm 25$  and  $150 \pm 30$  nm, respectively (see Fig. S2 of the ESM). Thus, carbon fiber microelectrodes were used.

Under the optimized mathematical calculations, the areas of the faradaic peak currents from the collisions are proportional to the sizes of the AgNPs. The resulted size distributions of nominal 10–20–40–60–100 nm AgNPs standard are shown in Fig. S6 of the ESM. The histograms of the sizes of the AgNPs from the silver standards follow a model of a Gaussian distribution around an average value. The intrinsic variability in the particle size are due, among other factors, to an incomplete oxidation of the nanoparticles during the time of the collisions, and the holistic simultaneous impact of two or more nanoparticles onto the electrode surface. These two factors produce spike currents with areas smaller or larger than those corresponding to the average value, respectively.

### Quantification of silver nanoparticles by the frequency of the nano-impacts

It has been demonstrated that the average number of stochastic particle impacts as a function of time on microelectrodes is diffusionally limited and is related to the number concentration of nanoparticles [23]. We have studied the application of the PCC for quantifying the AgNPs in samples in the presence of silver ions from the measurements of the frequency of the current spikes. It is expected that the frequency of the AgNPs-microelectrode collisions depends on the concentration of the AgNPs, besides the potential applied, the electrolyte identity (i.e., the diffusion coefficient of the AgNPs in the media), and the area of the microelectrode. The important thing is the number of current spikes, but not the area of these spikes. As explained in “PCC detection and size characterization of silver nanoparticles” section, a careful discrimination of the faradaic current peaks due to the nano-impacts with noise and faradaic currents is also necessary to obtain reliable data. In this sense, it is necessary to take into account the optimization of the mathematical treatments (the asymmetric factor of the baseline and threshold values, see additional information at the ESM).

The number of impacts was measured in 10 nm AgNPs suspensions in the range  $4.55 \times 10^5$  to  $4.55 \times 10^9$   $\text{L}^{-1}$  (c.a., in the range 0.0025 to 25  $\text{ng L}^{-1}$ ); using an optimized peak-height threshold of 0.0001 nA, a linear dependence of the number of impacts was observed at low concentrations, whereas the number of spikes tend to decrease at higher concentrations, losing this relationship. To study the cause of this behavior, the experimental data were fitted to different non-linear models in order to study generic trends based on the concentration. There were not found significant differences in the (linear/non-linear) curve fitting parameters calculated considering different time intervals along the chronoamperogram of 0.500–5.000 s, 5.001–10.000 s, and 4.000–10.000; the interval 0.500–5.000 s. was finally selected.

The experimental data was at first used for nonlinear curve fittings with a variety of appropriate curve fitting functions in

order to find the best model equation. Logarithm, exponential, power, and growing functions were tested to model the growing of the number of nano-impacts with the number of AgNPs in a high range of concentrations. The best nonlinear fittings found are summarized in Fig. 2: logarithm (Fig. 2a), exponential (Fig. 2b), growth (Fig. 2c), and power (Fig. 2d, e, f). At the 0.05 level, the allometric fitting function  $F(x) = a + bx^c$  (Fig. 2e) and the Belehradek fitting functions  $F(x) = a(x-b)^c$  (an x-shifted power function, Fig. 2f) are significantly better than the other functions, taking into account the adjusted *R*-square, the residual sum of the squares, and the reduced Chi-square of the functions. The same behavior of the Fig. 2 was observed with number of silver nanoparticles up to  $4.5 \times 10^{+8}$  ( $n = 5$  points) and up to  $4.5 \times 10^{+7} \text{ L}^{-1}$  ( $n = 4$  points). Relatively high concentrations of AgNPs are prone to aggregations and agglomerations over the time of the measurements, which can explain this behavior, together with changes in the electrolyte identity (i.e., in the diffusion coefficients of the AgNPs). The allometric2 fitting function is an extension of the classical Freundlich absorption model (an isotherm equation). This suggests the possible adsorption of the silver nanoparticles on the electrode surface at high concentrations.

In all cases, due to the small concentrations used, no double peaks due to aggregations of the AgNPs nor peaks with occasionally large areas (more than one spike at a time) were found. In a typical chronoamperogram of AgNPs (e.g., 40 nm diameter,  $0.025 \text{ ng mL}^{-1}$ ), the spikes have peak base width values of  $0.0070 \pm 0.0015 \text{ s}$  (mean  $\pm$  SD) and  $0.0050 \pm 0.0010 \text{ s}$  (median  $\pm$  SD). The full width at half maximum

height of the peak values were  $0.0016 \pm 0.0005 \text{ s}$  (mean  $\pm$  SD) and  $0.0012 \pm 0.0004 \text{ s}$  (median  $\pm$  SD) for the same chronoamperogram.

For quantification purposes, we have calculated a more convenient linear relationship dependence between the number of impacts and lower number concentrations of silver nanoparticles, which was obtained from ca.  $4.5 \times 10^5$  to  $4.5 \times 10^7 \text{ L}^{-1}$ . The linear relationship between the number of spikes and the concentration number of AgNPs (10 nm diameter) is shown in Fig. S7 of the ESM.

To evaluate the intra-assay precision in the quantification of the number of AgNPs based on this linear relationship, the number of current spikes produced between 0.500 and 10.000 s of a 20-nm standard AgNPs ( $1.14 \times 10^6 \text{ L}^{-1}$ , ca.  $0.050 \text{ ng L}^{-1}$  in  $0.020 \text{ M NaClO}_4$ ) were counted in replicate ( $n = 6$ ). A series of six chronoamperograms ( $E_e = +0.70 \text{ V}$ , up to 10 s) were recorded for a time of 12 min. The accumulated spike counts (0.5 to 10 s) were  $56 \pm 5$  ( $n = 6$ , %RSD = 8.9%). It was also observed that the number of impacts did not depend on the diameter of the NPs for a suitable threshold, but on the number concentration of these NPs. Standard AgNPs dispersions of 20 nm and 40 nm, both containing  $1.14 \times 10^6 \text{ L}^{-1}$  in  $0.020 \text{ M NaClO}_4$ , were analyzed in the same form ( $n = 6$ ). The results were  $58 \pm 5$  spikes (20 nm diameter) and  $55 \pm 5$  spikes (40 nm diameter). There was not significant difference between the two values ( $p = 0.05$ ). During the time of the chronoamperometric measurements, the frequency of collisions and the width of the peaks did not change significantly, indicating that there are no aggregations,

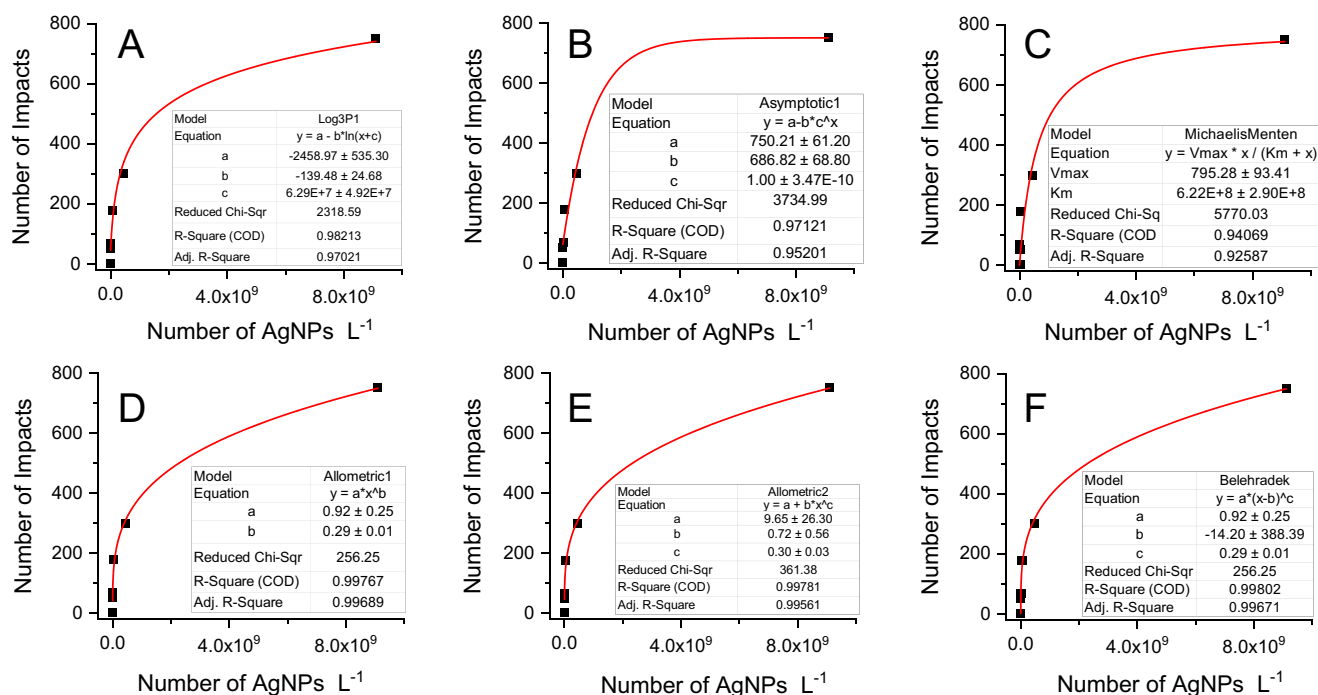


**Fig. 2** Nonlinear fittings of the function of the number on impacts (from 0.5 to 10 s) related to the number of silver nanoparticles  $\text{L}^{-1}$  (10 nm diameter). A total of 5 concentrations of AgNPs were measured in powers of 10 in the range  $4.5 \times 10^5$  to  $4.5 \times 10^8 \text{ L}^{-1}$

**Table 1** Summary of the determination of the AgNPs diameters in the three products measured by PCC, FESEM/TEM, and SP-ICP-MS. Values are expressed as mean  $\pm$  sd (nm) from 5 independent measurements ( $n = 5$ )

Sample	PCC	FESEM/TEM	SP-ICP-MS <sup>a</sup>
Wellness™	10.2 $\pm$ 1.3	9.0 $\pm$ 3.9	–
Biovedik™	14.5 $\pm$ 1.6	15.9 $\pm$ 5.5	–
High-Stability™	16.2 $\pm$ 1.5	18.9 $\pm$ 7.4	16.4 $\pm$ 3.4

<sup>a</sup> Due to the high concentrations of dissolved ionic silver, only silver nanoparticles larger than 21 nm (Wellness) and 45 nm (Biovecik) were measured by SP-ICP-MS

agglomerations, or adsorption of silver nanoparticles on the electrode in this time.

### Analysis of consumer products: comparison of methods

To study the applicability of the optimized PCC method to samples, the size distributions and the number concentration of AgNPs in three-silver colloidal products were analyzed. The size distribution results were compared with those measured with electron microscopy (FESEM, TEM) and SP-ICP-MS. The three samples were simply diluted with the

supporting electrolyte (NaClO<sub>4</sub> 0.02 M) before the electrochemical measurements, and with ultrapure water in SP-ICP-MS measurements, as explained in the experimental sections. The descriptive statistics of size distributions from electron microscopy and PCC methods are given in Figs. 3, 4, and 5. Table 1 summarizes the mean and standard deviation of the diameters calculated in these samples by the three techniques. The impacts used for the PCC size distribution determinations were those counted between 0.5 and 10 s.

The analysis of Wellness™ and Biovedik™ samples did not show accurate size distributions when measured by SP-ICP-MS because of the presence of high concentrations of silver ions (see Table 1), which resulted in high discrimination threshold, affecting the counting of nanoparticle events [24]. Consequently, small-sized nanoparticles were not detected, biasing actual size distributions for these samples to higher values than real ones. For this reason, high size detection limits of 21 and 45 nm were measured for the Wellness™ and Biovedik™ samples, respectively. This was not the case with the the High-Stability™ sample, with a lower concentration of Ag(I) (Table 2) and a size detection limit of 12 nm; the size distributions measured by SP-ICP-MS were in agreement with those measured by PCC and electron microscopy at the 95% level of confidence.

The number concentration of AgNPs in the three samples were determined by the optimized PCC method as explained in “[Optimization of the PCC procedure](#)” section. The results

**Fig. 3** Characterization of the Wellness™ sample. **a** TEM image. **b** Size distribution from TEM. **c** Chronoamperogram, sample diluted in NaClO<sub>4</sub> 0.02 M (1:10<sup>6</sup> (v/v), Inset: transient current spikes; and **d** Size's histogram measured by the PCC method

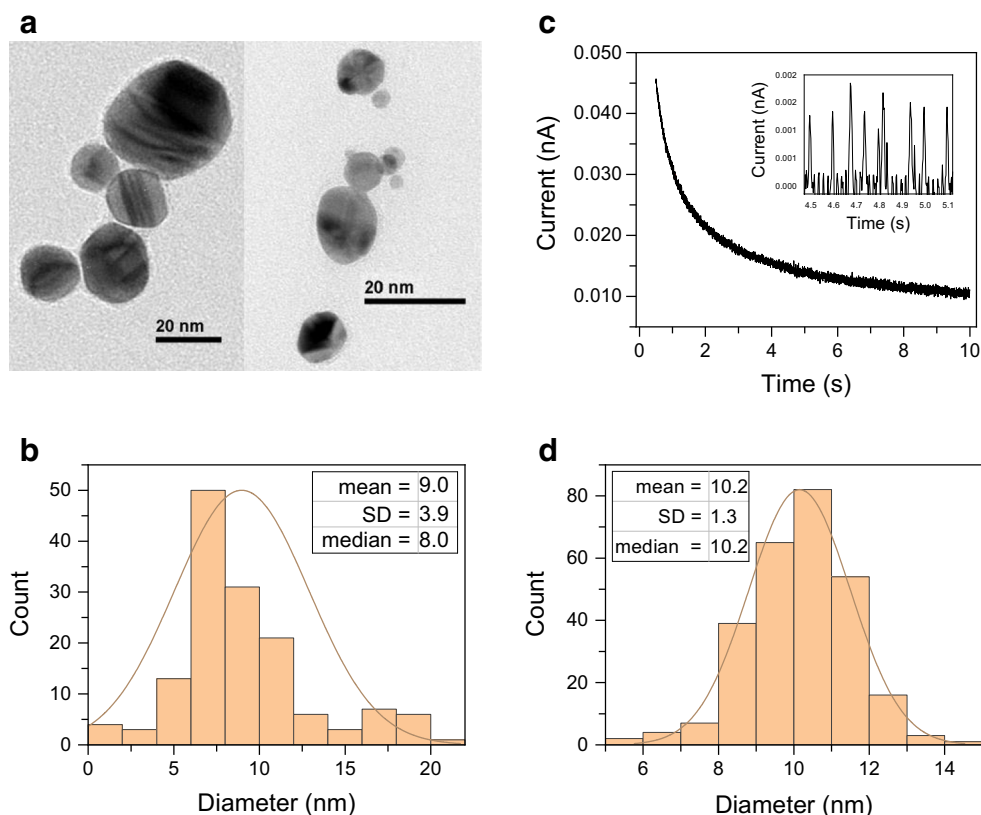
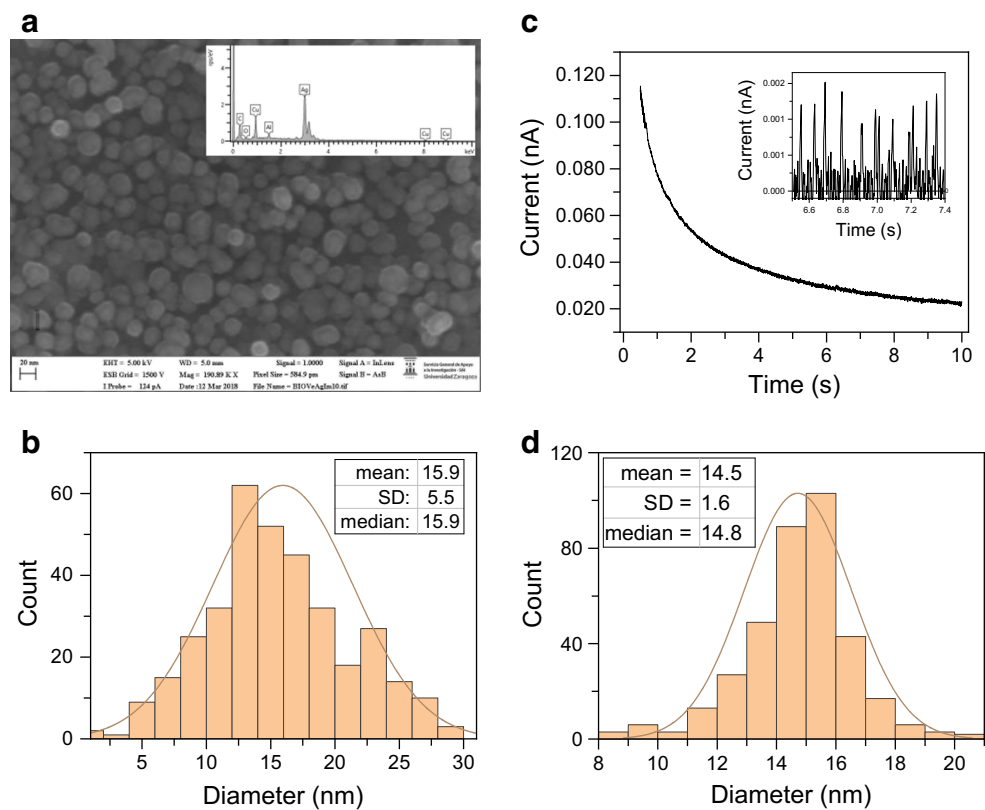


**Fig. 4** Characterization of the Biovedik™ sample. **a** FESEM image. Inset: X-ray spectrum showing silver detected by EDS; Cu and C peaks are due to a carbon-coated copper grid and Al peak comes from the aluminium sample holder. **b** Size distribution from the FESEM data. **c** Chronoamperogram, sample diluted in NaClO<sub>4</sub> 0.02 M. (1:10<sup>6</sup> (v/v), Inset of the transient current spikes. **d** Diameter's histogram measured by the PCC method



are summarized in Table 2, together with the concentrations of silver ions and the total silver in these samples measured by

AAS. The concentrations of dissolved Ag and total Ag are those measured by atomic absorption spectrometry in the

**Fig. 5** Characterization of the High-Stability™ sample diluted. **a** TEM image. **b** Size distribution measured by TEM. **c** Chronoamperogram, sample diluted in NaClO<sub>4</sub> 0.02 M (1:10<sup>6</sup> (v/v), Inset of the current transient spikes. **d** Diameter's distribution measured by the PCC method

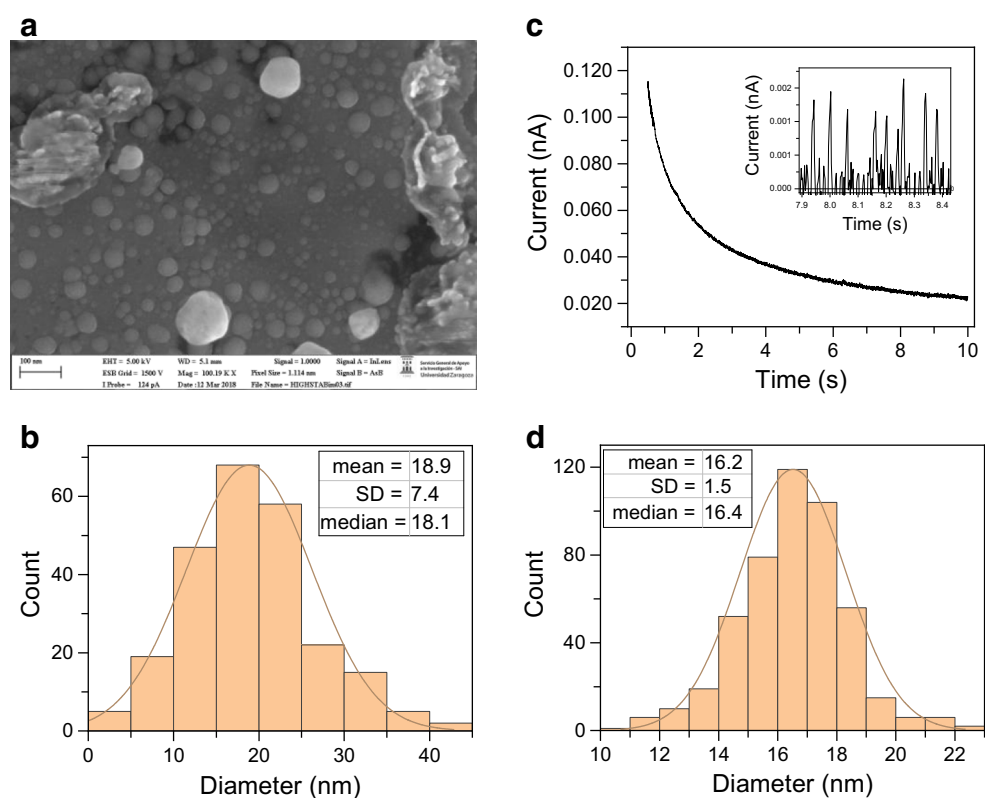




**Table 2** Summary of the results from the quantifications of AgNPs in the three consumer products by PCC, SP-ICP-MS, and AAS methods. All results are the mean  $\pm$  sd of  $n = 5$  independent determinations

Sample	PCC		SP-ICP-MS		AAS	
	AgNP, L <sup>-1</sup>	AgNP, mg Ag L <sup>-1</sup>	AgNP, L <sup>-1</sup>	AgNP, mg Ag L <sup>-1</sup>	Dissolved <sup>a</sup> Ag, mg L <sup>-1</sup>	Total Ag, mg L <sup>-1</sup>
Wellness™						
Biovedik™	$2.4 \pm 0.2 \times 10^7$	$16.4 \pm 2.0$	–	–	$15.0 \pm 0.9$	$32.3 \pm 0.2$
High-stability™	$1.9 \pm 0.3 \times 10^7$	$14.4 \pm 1.5$	–	–	$7.1 \pm 0.5$	$20.9 \pm 0.5$
Sample	$1.0 \pm 0.4 \times 10^7$	$11.6 \pm 1.0$	$1.72 \pm 0.2 \times 10^{12}$	$10.6 \pm 1.3$	$0.4 \pm 0.1$	$12.1 \pm 0.3$

<sup>a</sup> Determined after ultrafiltration (cut-off 3 kDa)

ultrafiltered samples (3-kDa pore size diameter) and without ultrafiltration, respectively. The quantification of nanoparticle number concentrations by the PCC method ( $1.0 \pm 0.4 \times 10^7$ ) showed results in fair agreement with those measured by SP-ICP-MS for the High-Stability™ sample ( $1.72 \pm 0.15 \times 10^{12}$  L<sup>-1</sup>) taking into the account the different dilutions of the samples (about  $1/10^{7.7}$  and  $1/10^{2.5}$  (v/v) in PCC and SP-ICP-MS, respectively). In the three samples, the concentrations for the diameter of the silver nanoparticles measured by PCC were in agreement with those of the difference between the total silver and the Ag(I) concentrations measured by AAS.

In conclusion, the PCC method allowed to determine size distributions of AgNPs and number concentration of nanoparticles in samples in the presence of significant concentrations of silver ions, especially with small nanoparticles having diameters of the order of 10 nm. On the other hand, the SP-ICP-MS method gave accurate results only with diameters higher than 20–45 nm when significant Ag(I) was present in the samples. The PCC method also produced better results with very small diameters, in which the kinetics of the electron transfer and the complete oxidation of the AgNPs is favored. Statistical analysis (two sample *t* test,  $p < 0.05$ ) did not report significant difference between TEM/FESEM and PCC average diameters at the 95% confidence level in the three samples studied.

## Conclusions

The developed PCC method allows the detection of AgNPs, size characterization, and the quantification of the number concentration of nanoparticles in consumer products, in the presence of significant amounts of Ag(I) ions. The sizes of the nominal 10–100 nm diameter standard AgNPs were comparable to those obtained with electron microscopy. Nevertheless, for obtaining accurate results, the mathematical treatments of the voltammetric data have to be carefully optimized, mainly in the subtraction of the current baseline and the discrimination of the faradaic and noisy currents with

threshold values, since they have a significant influence on the analytical results obtained.

An allometric and Belehradek power functions were demonstrated in the fitting of the frequency of the electrochemical collisions with the number of the nanoparticles, which suggest adsorption of the silver nanoparticles on the electrode during the timescale of the measurements at relatively high concentrations. The precise quantification of the number of nanoparticles can be estimated in very diluted concentrations, in which there is a linear relationship with the number of accumulated electrochemical spikes. This relationship allows to the sensitive quantification of the number of silver nanoparticles in colloidal silver consumer products. The size distributions of silver nanoparticles analyzed by the PCC method are in agreement with those measured by electron microscopy in the three studied consumer samples. The PCC method is particularly more useful than the SP-ICP-MS method with the smallest AgNPs (10–20 nm) and in the presence of high concentrations of dissolved silver.

**Supplementary Information** The online version contains supplementary material available at <https://doi.org/10.1007/s00604-020-04662-4>.

**Funding** This work has been supported by the Ministry of Science, Innovation, and Universities and the European Regional Development Fund project RTI2018-096111-B-I00 (MICINN/FEDER) and by the Government of Aragon (E29\_17R), and co-financed with FEDER 2014-2020. The work has been also 65% cofinanced by the European Regional Development Fund (ERDF) through the Interreg VA Spain-France-Andorra programme (POCTEFA 2014-2020), Project OUTBIOTICS EFA183/16.

## Compliance with ethical standards

**Conflict of interest** The authors declare that they have no conflict of interest.

## References

- Haider A, Kang IK (2015) Preparation of silver nanoparticles and their industrial and biomedical applications: a comprehensive review. *Adv Mater Sci Eng* 2015:1–16. <https://doi.org/10.1155/2015/165257>

2. Zhang W, Xiao B, Fang T (2018) Chemical transformation of silver nanoparticles in aquatic environments: mechanism, morphology and toxicity. *Chemosphere* 191:324–334. <https://doi.org/10.1016/j.chemosphere.2017.10.016>
3. Marambio-Jones C, Hoek EMV (2010) A review of the antibacterial effects of silver nanomaterials and potential implications for human health and the environment. *J Nanopart Res* 12:1531–1551. <https://doi.org/10.1007/s11051-010-9900-y>
4. Bhatt I, Tripathi BNI (2011) Interaction of engineered nanoparticles with various components of the environment and possible strategies for their risk assessment. *Chemosphere* 82:308–317. <https://doi.org/10.1016/j.chemosphere.2010.10.011>
5. Stebounova LV, Guio E, Grassian VH (2011) Silver nanoparticles in simulated biological media: a study of aggregation, sedimentation, and dissolution. *J Nanopart Res* 13:233–244. <https://doi.org/10.1007/s11051-010-0022-3>
6. Laborda F, Bolea E, Cepriá G, Gómez MT, Jiménez MS, Pérez-Arategui J, Castillo JR (2016) Detection, characterization and quantification of inorganic engineered nanomaterials: a review of techniques and methodological approaches for the analysis of complex samples. *Anal Chim Acta* 904:10–32. <https://doi.org/10.1016/j.aca.2015.11.008>
7. Calzolari L, Gilliland D, Rossi F (2012) Measuring nanoparticles size distribution in food and consumer products: a review. *Food Addit Contam Part A Chem Anal Control Expo Risk Assess* 29: 1183–1193. <https://doi.org/10.1080/19440049.2012.689777>
8. Laborda F, Bolea E, Jiménez-Lamana J (2014) Single particle inductively coupled plasma mass spectrometry: a powerful tool for nanoanalysis. *Anal Chem* 86:2270–2278. <https://doi.org/10.1021/ac402980q>
9. Batchelor-McAuley C, Käthelön E, Barnes EO, Compton RG, Laborda E, Molina A (2015) Recent advances in voltammetry. *ChemistryOpen* 4:224–260. <https://doi.org/10.1002/open.201500042>
10. Bettazi F, Palchetti I (2019) Nanotoxicity assessment: a challenging application for cutting edge electroanalytical tools. *Anal Chim Acta* 1072:61–74. <https://doi.org/10.1016/j.aca.2019.04.035>
11. Cheng W, Compton RG (2014) Electrochemical detection of nanoparticles by ‘nano-impact’ methods. *TrAC Trends Anal Chem* 58: 79–89. <https://doi.org/10.1016/j.trac.2014.01.008>
12. Stuart EJE, Zhou YG, Rees NV, Compton RG (2012) Determining unknown concentrations of nanoparticles: the particle-impact electrochemistry of nickel and silver. *RSC Adv* 2:6879–6884. <https://doi.org/10.1039/C2RA20628E>
13. Rees NV (2014) Electrochemical insight from nanoparticle collisions with electrodes: a mini-review. *Electrochem Commun* 43:83–86. <https://doi.org/10.1016/j.elecom.2014.03.018>
14. Zhou YG, Rees NV, Compton RG (2011) The electrochemical detection and characterization of silver nanoparticles in aqueous solution. *Angew Chem* 50:4219–4221. <https://doi.org/10.1002/anie.201100885>
15. Stuart EJE, Rees NV, Cullen JT, Compton RG (2013) Direct electrochemical detection and sizing of silver nanoparticles in seawater media. *Nanoscale* 5:174–177. <https://doi.org/10.1039/C2NR33146B>
16. Boika A, Bard AJ (2015) Time of first arrival in electrochemical collision experiments as a measure of ultra low concentrations of analytes in solution. *Anal Chem* 87:4341–4346. <https://doi.org/10.1021/acs.analchem.5b00037>
17. Sokolov SV, Bartlett TR, Fair P, Fletcher S, Compton RG (2016) Femtomolar detection of silver nanoparticles by flow-enhanced direct-impact voltammetry at a microelectrode array. *Anal Chem* 88: 8908–8912. <https://doi.org/10.1021/acs.analchem.6b02670>
18. Rees NV, Zhou YG, Compton RG (2011) The aggregation of silver nanoparticles in aqueous solution investigated via anodic particle coulometry. *ChemPhysChem* 12:1645–1647. <https://doi.org/10.1002/cphc.201100207>
19. Hernández D, Cepriá G, Laborda F, Castillo JR (2019) Detection and determination of released ions in the presence of nanoparticles: selectivity or strategy? *Electroanalysis* 31:405–410. <https://doi.org/10.1002/elan.201800597>
20. Ngamchuea K, Clark ROD, Sokolov SV, Young NP, Batchelor-McAuley C, Compton RG (2017) Single oxidative collision events of silver nanoparticles: understanding the rate-determining chemistry. *Chem Eur J* 23:16085–16096. <https://doi.org/10.1002/chem.201703591>
21. Little CA, Xie R, Batchelor-McAuley C, Käthelön E, Li X, Young NP, Compton RG (2018) A quantitative methodology for the study of particle-electrode impacts. *Phys Chem Chem Phys* 20:13537–13546. <https://doi.org/10.1039/C8CP01561A>
22. Toh HS, Jurkschat K, Compton RG (2015) The influence of the capping agent on the oxidation of silver nanoparticles: nano-impacts versus stripping voltammetry. *Chem Eur J* 21:2998–3004. <https://doi.org/10.1002/chem.201406278>
23. Eloul S, Käthelön E, Batchelor-McAuley C, Tschulik K, Compton RG (2015) Diffusional impacts of nanoparticles on microdisc and microwire electrodes: the limit of detection and first passage statistics. *J Electroanal Chem* 755:136–142. <https://doi.org/10.1016/j.jelechem.2015.07.042>
24. Abad-Álvaro I, Peña-Vázquez E, Bolea E, Bermejo-Barrera P, Castillo JR, Laborda F (2016) Evaluation of number concentration quantification by single-particle inductively coupled plasma mass spectrometry: microsecond vs. millisecond dwell times. *Anal Bioanal Chem* 408:5089–5097. <https://doi.org/10.1007/s00216-016-9515-y>

**Publisher's note** Springer Nature remains neutral with regard to jurisdictional claims in published maps and institutional affiliations.